JACS
JOURNAL OF THE AMERICAN CHEMICAL SOCIETY
Article
pubs.acs.org/JACS

Photogenerated Charge Carriers and Reactive Oxygen Species in ZnO/Au Hybrid Nanostructures with Enhanced Photocatalytic and Antibacterial Activity

Weiwei He,[†,‡] Hyun-Kyung Kim,[‡,§] Wayne G. Wamer,[‡] David Melka,[‡] John H. Callahan,[‡] and Jun-Jie Yin*[,‡]

[†]Key Laboratory of Micro-Nano Materials for Energy Storage and Conversion of Henan Province, Institute of Surface Micro and Nano Materials, Xuchang University, Henan 461000, P. R. China

[‡]Center for Food Safety and Applied Nutrition, U.S. Food and Drug Administration, College Park, Maryland 20740, United States

[§]Food Safety Bureau, Ministry of Food and Drug Safety, Osong Health Technology Administration Complex 363-700, Republic of Korea

Supporting Information

ABSTRACT: Semiconductor nanostructures with photocatalytic activity have the potential for many applications including remediation of environmental pollutants and use in antibacterial products. An effective way for promoting photocatalytic activity is depositing noble metal nanoparticles (NPs) on a semiconductor. In this paper, we demonstrated the successful deposition of Au NPs, having sizes smaller than 3 nm, onto ZnO NPs. ZnO/Au hybrid nanostructures having different molar ratios of Au to ZnO were synthesized. It was found that Au nanocomponents even at a very low Au/ZnO molar ratio of 0.2% can greatly enhance the photocatalytic and antibacterial activity of ZnO. Electron spin resonance spectroscopy with spin trapping and spin labeling was used to investigate the enhancing effect of Au NPs on the generation of reactive oxygen species and photoinduced charge carriers. Deposition of Au NPs onto ZnO resulted in a dramatic increase in light-induced generation of hydroxyl radical, superoxide and singlet oxygen, and production of holes and electrons. The enhancing effect of Au was dependent on the molar ratio of Au present in the ZnO/Au nanostructures. Consistent with these results from ESR measurements, ZnO/Au nanostructures also exhibited enhanced photocatalytic and antibacterial activity. These results unveiled the enhanced mechanism of Au on ZnO and these materials have great potential for use in water purification and antibacterial products.

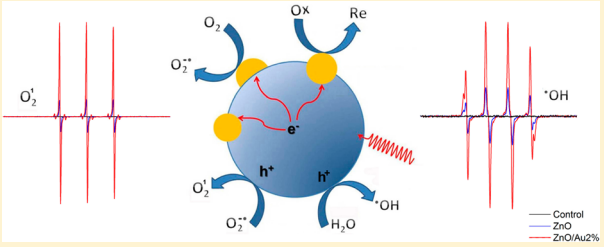

INTRODUCTION

Because of their current and potential commercial importance, nanomaterials composed of metal oxides have received a great deal of interest. Metal oxide nanomaterials, such as ZnO and TiO_2, have been used in sunscreens,[1] antimicrobial agents,[2,3] solar energy conversion, and photocatalysis for remediation of environmental pollutants.[4−6] The unique way in which metal oxide nanomaterials interact with light underlies many of these applications. When light (usually UV light) is absorbed, the photoexcited nanoparticle stores energy by charge separation and creating electron−hole pairs. The fate of the electron/hole pairs determines the chemical and biological reactivity of the photoexcited nanoparticle. Pure semiconductors usually exhibit low photoenergy conversion efficiency probably because of their relatively low charge separation efficiency and fast recombination of charge carriers.[7] Recently, the combination of metal oxide NPs with noble metals to form metal/semiconductor hybrid nanostructures has been proposed as a way to increase photocatalytic efficiency.[8−10] For example, deposition of Au or Pt NPs onto TiO_2 was reported to greatly improve the photocatalytic reaction rate in organic degradation reactions.[11] The preparation and enhanced photcatalytic activity of noble metal/metal oxide hybrid nanostructures have been reported.[12−14] Noble metal NPs have been shown to increase the photoenergy conversion efficiency of semiconductors by (1) increasing the efficiency of charge carrier separation,[11,15] and (2) extending light absorption and facilitating creation of electron/hole pairs induced by the surface plasmon resonance (SPR) effect (especially for Au and Ag).[16−18] However, optimizing the efficiency of noble metal/metal oxide nanostructures remains a challenge because of our limited understanding of the mechanisms by which noble metals alter the fundamental photophysics (e.g., effects on charge carrier lifetime) and photochemistry (e.g., generation of reactive chemical intermediates) of metal oxides.

Reactive oxygen species (ROS), typically including hydroxyl radicals, singlet oxygen and superoxide radicals, have been proposed as the main reactive species responsible for the photocatalytic activity of semiconductor NPs.[19,20] Similarly,

Received: October 25, 2013
Published: December 19, 2013

   dx.doi.org/10.1021/ja410800y | J. Am. Chem. Soc. 2014, 136, 750−757

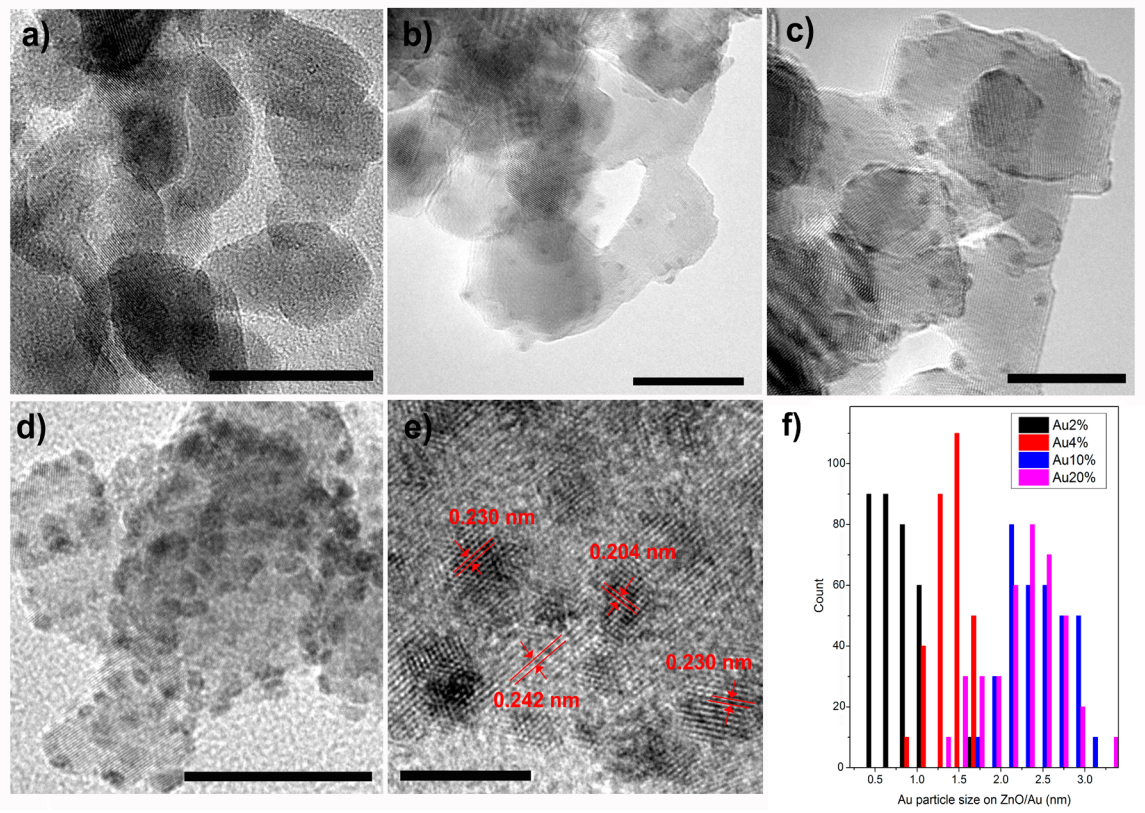

Figure 1. TEM images of ZnO NPs (a) and ZnO/Au hybrid NPs formed at different Au/ZnO molar ratios of 0.02 (b), 0.04 (c), and 0.1 (d). (e) HRTEM image for the sample from panel d; (f) size distribution of Au particles formed on ZnO at different molar ratios for reactants. Scale bars in panels a–d are all 20 nm; scale bar in panel e is 5 nm.

generation of ROS, resulting in oxidative stress, has been recognized as a predominant mechanism underlying the effects of photoexcited metal oxides on mammalian and bacterial cells.[21,22] In addition, physical interaction with cellular components and metal ions released following dissolution appear to contribute to the bioactivity of some metal oxides.[23,24] Zhang et al. have proposed that the band gap energy can be used to rank the ability of metal oxide NPs to induce oxidative stress and biological responses such as acute inflammation.[25] A number of mechanistic studies have investigated the events following photoexcitation of NPs leading to generation of ROS. Investigators have used indirect spectroscopy or electron spin resonance (ESR) spectroscopy to determine the generation of ROS,[26,27] and transient spectroscopic methods to measure charge carrier dynamics.[28] However, detailed mechanistic studies on noble metal/metal oxide NPs are very limited. As a result, we lack the knowledge needed to optimize the photocatalytic and antibacterial activities of these NPs.

ESR spectroscopy is a powerful tool for studying molecules and materials with unpaired electrons.[29] ESR with spin trapping is the most reliable and direct method for identification and quantification of short-lived free radicals. Spin trapping is based on the reaction between an unstable free radical and the spin trap to produce a relatively stable spin adduct, which is then characterized by ESR. Spin trapping has been used to detect free radical intermediates in photoinduced reactions involving semiconductors such as TiO_2 and ZnO.[30] However, it is difficult to identify photoinduced charge carriers (electrons and holes) using spin trapping. Recently, 2,2,6,6-tetramethylpiperidine-1-oxyl (TEMPO) has been employed as a NMR probe for elucidation of electron and proton transfer during photoexcitation of TiO_2 and ZnO.[31] This application inspired us to investigate the utility of TEMPO and ESR to examine the effect of metal NPs on electrons and holes formed during photoexcitation of semiconductors. Combined use of ESR spin traps and spin probes can give detailed mechanistic information about both the generation of ROS and behavior of electron/hole pairs.

In this study, we examined ZnO/Au hybrid nanostructures as an example of metal oxide/noble metal nanostructures. Zinc oxide was selected as a representative metal oxide because of its widespread use in commercial products. Our primary objective in studying ZnO/Au hybrid nanostructures was to understand the relationships among charge carrier formation, generation of reactive intermediates, photocatalytic activity, and antibacterial activity. An additional objective was to determine how the amount of Au loaded into a ZnO/Au hybrid nanoparticle determines its photochemical reactivity and antibacterial behavior. In assessing the effect of Au NPs on the generation of ROS, it is critical to develop methods for definitively identifying each ROS. Therefore in this work, we also have developed methods using ESR spectroscopy with spin trapping and spin probes to identify and quantify individual ROS formed following photoexcitation of ZnO and ZnO/Au hybrid nanostructures.

RESULTS AND DISCUSSION

Formation of ZnO/Au Hybrid Nanostructures. ZnO/Au hybrid nanostructures were synthesized by the photoreduction method, in which photoinduced electrons from ZnO were employed to reduce $AuCl_4^-$ (Au^{3+}) on the ZnO surface. This method has two advantages: (1) very small particles of Au (<3

dx.doi.org/10.1021/ja410800y | J. Am. Chem. Soc. 2014, 136, 750–757

nm) are obtained, and (2) this method is environmentally friendly and low cost because it needs no additional reactants. Figure 1 displays the TEM images of pure ZnO NPs and ZnO/Au hybrid nanostructures having different amounts of Au loading. Commercial ZnO NPs have an irregular shape with a diameter of about 30 nm. During photoreduction of Au^{3+} in the presence of ZnO NPs, the original white suspension changed to dark gray indicating formation of ZnO/Au. Figure 1 panels b and c clearly show the dark Au dots distributed on the surface of ZnO. We observed this color change even during reactions involving reactants at the lowest molar ratio (0.2%) of $HAuCl_4$ to ZnO. The product of this reaction is referred to as ZnO/Au0.2%. However, at this level of Au deposition, no Au NPs are visible on the surface of ZnO. Here, the Au clusters deposited on ZnO may be too small for observation by TEM. Dots are visible in TEM images for ZnO/Au hybrid nanostructures formed during reaction of $HAuCl_4$ and ZnO at a molar ratio of 0.02 (ZnO/Au2%, Figure 1b). When the molar ratio for reactants is increased, both the size and density of Au dots significantly increase (Figure 1c,d). We have calculated the Au dot size for reactions using different molar ratios of $HAuCl_4$ and ZnO. The size distribution is shown in Figure 1f. We found that the average size was 0.77 (±0.2), 1.4 (±0.2) and 2.3 (±0.4) nm corresponding to reactant molar ratios ($HAuCl_4$ to ZnO) of 0.02, 0.04 and 0.1, respectively. The size of Au dots formed when the reactant molar ratio was further increased to 0.2 was 2.4 ± 0.3 nm (Figure 1f). This indicates that no significant increase in the size of deposited Au dots is associated with larger molar ratios of $HAuCl_4$ to ZnO. Energy dispersive X-ray (EDX) analysis confirms the coexistence of Au and Zn in the hybrid nanostructures (Supporting Information, Figure S1). Assuming a complete conversion of $AuCl_4^-$ to Au, we compared the calculated Au/Zn ratios with the measured ratios (from EDX analysis, average of three measurements). We found a linear relationship with a slope of 0.29. This linear relationship indicates that the molar percentage of Au deposited on ZnO is proportional to the molar percentage of $AuCl_4^-$ in the reaction mixture. Because the slope for the linear relationship is less than 1, it is clear that not all (~ 30%) of the $AuCl_4^-$ is photoreduced and deposited onto ZnO as Au dots. Overall, these results indicate that loading of Au onto ZnO can be controlled simply by changing the molar ratio of reactants.

The high resolution TEM (HRTEM) image clearly shows the lattice pattern and indicates that Au dots have a single crystalline structure (Figure 1e). For Au dots, lattice spacing was calculated to be 0.230 and 0.204 nm, which is similar to the planar distance for Au {111} (0.235 nm) and Au {200} (0.204 nm), respectively. The *d* spacing from ZnO is 0.242 nm corresponding to the hexagonal ZnO {101} plane (0.246 nm). It was noteworthy that Au deposits as nanoislands on ZnO rather than as a smooth Au shell, even at higher molar ratios of Au. This is due to the large difference in crystal lattice between Au and ZnO. We also noted that Au {111} faces preferred to grow on ZnO {101} planes. This may be attributed to the relatively small lattice mismatch (4.47%) between Au {111} and ZnO {101} facets. The XRD pattern further supports the formation of ZnO/Au hybrid structures (Figure 2). The diffraction peaks from pure ZnO samples can be indexed to the hexagonal phase of the zincite structure (JCPDS NO. 1-1136), with no additional impurity peaks. After deposition of Au at a reactant molar ratio of 2% Au/ZnO, the typically strong peak of Au (111) and weak Au (200) indicate the formation of crystalline Au, and the dominantly exposed faces are consistent with the HRTEM observation. The specific surface

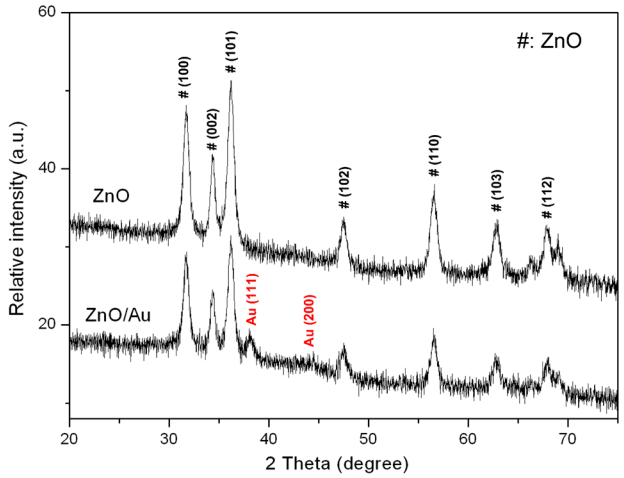

Figure 2. X-ray diffraction (XRD) pattern of ZnO NPs and ZnO/Au hybrid nanostructures obtained at a Au/ZnO molar ratio for reactants of 2%.

areas (SSA) for ZnO, ZnO/Au hybrid nanostructures with different Au/ZnO molar ratios of 0.2%, 2%, and 10%, are determined to be 63.02, 49.35, 46.44, and 36.30 m^2/g, respectively, which indicates the reduction of SSA with an increase of the Au loading on ZnO.

Au NPs are often employed to improve the optical and catalytic properties of metal or semiconductor nanomaterials, because of their unique SPR properties. The SPR property is highly dependent on the size and shape of Au NPs. As reported, Au particles smaller than 3 nm show negligible SPR phenomena.[32] To determine how depositing small Au dots affects the optical properties of ZnO, we examined the UV−vis spectra of ZnO suspensions before and after modification with Au dots (Supporting Information, Figure S2). Even at a very low Au/ZnO ratio of 0.002, deposition of Au onto ZnO significantly influenced the optical response of ZnO. We observed a stronger adsorption intensity below 350 nm and an absorption edge shift to shorter wavelength. The band gap energy (E_g) was calculated based on the absorption spectra by the formula, $\alpha h\nu = A(h\nu - E_g)^{1/2}$, where α is the absorption coefficient, A is a constant, $h\nu$ is the photon energy. Deposition of Au resulted in an about a 10% increase in the band gap (Supporting Information, Figure S2 inset). Increasing the Au/ZnO ratio further resulted in no additional changes in the spectra and/or band gap. Also, none of the spectra show a SPR absorption band characteristic for Au NPs around 520 nm. This may be because the SPR effect is very weak for small Au dots.

Enhanced Effect of Au Loading on Photocatalytic Degradation over ZnO/Au NPs. ZnO has been studied extensively because of its high photocatalytic activity. We examined how Au deposition affected the photocatalytic performance of ZnO. The photocatalytic activity of ZnO and various ZnO/Au hybrid nanostructures have been evaluated by degradation of two representative substrates, the organic dye methylene blue (MB) and the colorless pollutant salicylic acid (SA) (Figure 3). ZnO NPs show good catalytic ability both for the degradation of MB and SA under simulated sunlight. After Au modification even at a very low Au/ZnO molar ratio of 0.002, the degradations of MB and SA were both significantly enhanced. Moreover, ZnO/Au with a higher Au to ZnO molar ratio exhibited enhanced photocatalytic performance. For example, ZnO/Au hybrid nanostructures at Au to ZnO molar ratio of 0.1

dx.doi.org/10.1021/ja410800y | J. Am. Chem. Soc. 2014, 136, 750−757

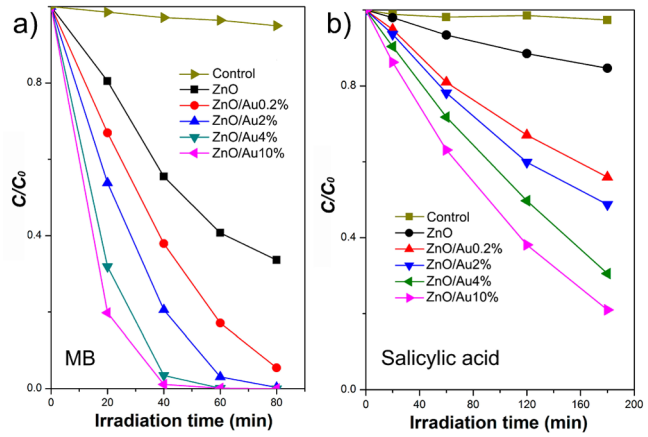

Figure 3. Photocatalytic activity of ZnO and ZnO/Au NPs with different Au loading on the degradation of MB (a) and SA (b) under simulated sunlight. The concentration of catalysts is fixed at 0.1 mg/mL.

have a photocatalytic activity about four times higher than ZnO at 20 min toward the MB degradation. These observations verify that deposition of Au onto ZnO significantly enhances the photocatalytic activity of ZnO.

Reactive oxygen species and photogenerated charge carriers have been proposed as the main reactive species responsible for the reactions photocatalyzed by ZnO. Therefore, we examined how the deposition of Au onto ZnO influenced the generation of ROS and behavior of charge carriers. For this purpose, it was critical to develop a method to identify and distinguish the ROS and photogenerated holes and electrons. We have used ESR spectroscopy with spin trapping and labeling as an effective technique to identify and characterize the activities of the ROS and electron/holes generated during irradiation of ZnO/Au hybrid nanostructures.

Identification of ROS and Charge Carriers by ESR Spectroscopy. ESR spin trapping and spin labeling are two recognized techniques for the detection of short-lived free radicals and paramagnetic species.[33] Spin labels refer to the molecules with unpaired electrons and having an ESR signal, for example, TEMPO. Silent spin labels are molecules which are ESR silent but form stable radicals with an ESR signal after donating electrons, for example, 2,2,6,6-tetramethylpiperidine (TEMP) and 1-hydroxy-3-carboxy-2,2,5,5-tetramethylpyrrolidine (CPH). Generally, the silent spin labels are the reduced state of spin labels. Here, we select 5-tertbutoxycarbonyl-5-methyl-1-pyrroline *N*-oxide (BMPO) as a spin trap for the hydroxyl radical and superoxide, 4-oxo-2,2,6,6-tetramethylpiperidine (4-oxo-TEMP) for detection of singlet oxygen, and TEMPO and CPH for characterization of electrons and holes. In addition, for confirmation of each ROS, we examined the scavenging of the hydroxyl radical, superoxide, and singlet oxygen by DMSO, superoxide dismutase (SOD), and NaN_3, respectively. Figure 4 illustrates the method used in this study to identify and distinguish the reactive species formed during photoexcitation of ZnO and ZnO/Au hybrid nanostructures.

Figure 5 shows the ESR spectra obtained from solutions containing various spin probes and ZnO or ZnO/Au hybrid nanostructures before and during irradiation with simulated sunlight. No ESR signal was observed for control samples (unirradiated samples or samples without catalysts for BMPO, 4-oxo-TEMP or CPH). First, BMPO was chosen to verify the generation of hydroxyl radicals and superoxide induced by ZnO and ZnO/Au. Upon irradiation for 5 min in the presence of ZnO,

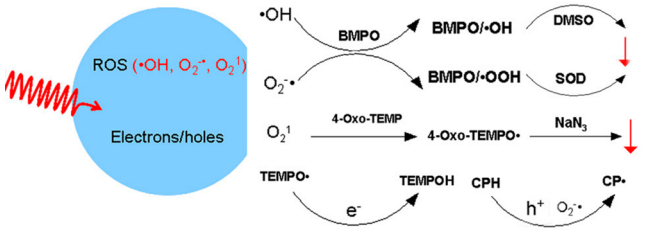

Figure 4. Methods used to distinguish the ROS and charge carriers formed during photoexcitation of ZnO and ZnO/Au. The downward arrow represents the decrease of corresponding products.

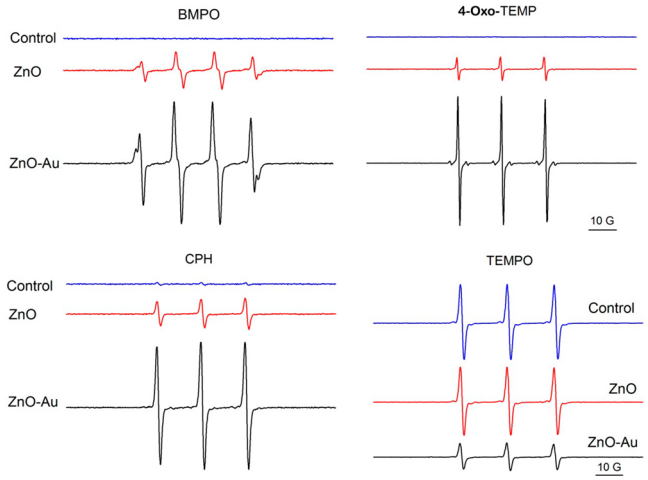

Figure 5. Significant enhancement effect of Au in ZnO/Au hybrid nanostructures for generation of ROS and charge carriers under simulated sunlight. ESR spectra obtained from samples containing different spin probes (25 mM BMPO, 0.02 mM CPH, 2 mM 4-Oxo-TEMP or 0.02 mM TEMPO) and 0.1 mg/mL ZnO or ZnO/Au2% NPs. The control represents the sample containing spin probe alone under simulated sunlight, and the sample containing spin probe and catalysts before exposure to simulated sunlight. All the spectra were recorded after 5 min of irradiation with simulated sunlight.

we clearly observed a four-line spectrum with relative intensities of 1:2:2:1 and hyperfine splitting parameters of $a_N = 13.56$, $a^{\beta}_H = 12.30$, $a^{\gamma}_H = 0.66$, which is the characteristic spectrum for the adduct formed between BMPO and the hydroxyl radical (BMPO/·OH).[34] When ZnO/Au2% hybrid nanostructures were added, the BMPO/·OH signal intensity increased significantly (about 4 times). These results indicate that the hydroxyl radical is generated by ZnO and ZnO/Au during irradiation and that deposition of Au onto ZnO significantly enhances photogeneration of hydroxyl radicals. BMPO is also a spin trap frequently used for capturing superoxide. While no characteristic ESR signal for the adduct formed between BMPO and superoxide (BMPO/·OOH) was observed, BMPO/·OH and BMPO/·OOH have overlapping ESR spectra. To determine whether the ESR signal in part comes from the superoxide, we investigated the scavenging effect of DMSO and SOD on the ESR signal from ZnO and ZnO/Au (Supporting Information, Figure S3). DMSO and SOD are efficient and specific scavengers for the hydroxyl radical and superoxide, respectively. For comparison, superoxide was produced through a classic enzymatic system, xanthine/XOD. When xanthine/XOD was the source of superoxide, DMSO had no effect on the ESR spectrum for the BMPO/·OOH spin adduct. As expected, no ESR signal was observed for BMPO/·OOH in the presence of

dx.doi.org/10.1021/ja410800y | J. Am. Chem. Soc. 2014, 136, 750−757

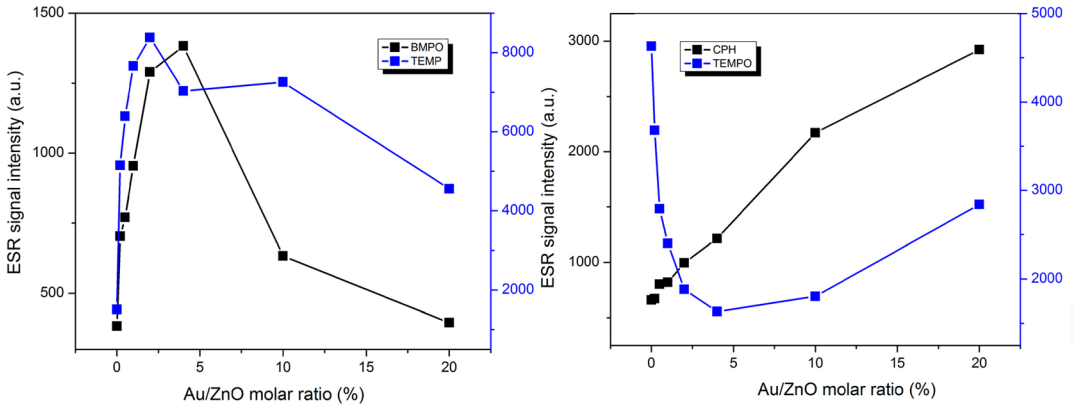

Figure 6. Effect of Au loading on the enhancement of ROS generation during irradiation.

SOD. When photoexcited ZnO or ZnO/Au were the sources for radical generation, we found that (1) the addition of 10% DMSO leads to significant reduction of hydroxyl radical and the residual signal can be assigned to BMPO/·OOH adduct (marked in asterisk in Supporting Information, Figure S3), and (2) the addition of 0.25 U/mL SOD also partly inhibits the ESR signal, indicating the involvement of the superoxide. These results indicate that both hydroxyl radical and superoxide are generated during irradiation of ZnO and ZnO/Au nanostructures.

In addition to the hydroxyl radical and superoxide, singlet oxygen is another important ROS. 4-Oxo-TEMP was selected as a spin probe for investigating the enhancing effect of Au on singlet oxygen generation. 4-Oxo-TEMP itself is ESR silent. No ESR signal was observed for samples containing the spin probe and ZnO without irradiation or the irradiated spin probe alone. A triplet spectrum, characteristic for the reaction between the spin probe and singlet oxygen, was observed during irradiation of either ZnO or ZnO/Au hybrid nanostructures (Figure 5). This ESR spectrum verifies the production of singlet oxygen. To confirm that the ESR signal resulted from singlet oxygen, the effect of sodium azide, a singlet oxygen scavenger, was tested. The triplet ESR spectrum was reduced greatly when ZnO or ZnO/Au were irradiated in the presence of sodium azide, thus confirming the previous observation of the production of singlet oxygen (Supporting Information, Figure S4). For the same amount and recording time, the ESR signal intensity generated from photoexcited ZnO/Au2% is calculated as about 7 times the signal from pure ZnO, indicating that deposition of Au on ZnO greatly enhanced generation of singlet oxygen.

CPH, though ESR silent itself, can be oxidized to form CP-nitroxide (CP·) radicals with a typical ESR spectrum of three lines with intensity ratios of 1:1:1. CPH is not a specific spin label since it may react with a number of oxidants such as ROS and holes generated as charge carriers in photocatalysts. Therefore, CPH was employed here to determine the overall photo-oxidative behavior caused by holes and ROS. CPH can be very slowly oxidized to form nitroxides by dissolved oxygen or irradiation. When CPH is exposed to simulated sunlight in the presence of ZnO or ZnO/Au, we observe ESR spectra consisting of three-lines with hyperfine splitting constant a_N = 16.2 G. Parallel observations were made for the generation of hydroxyl radical and singlet oxygen; the ESR signal is approximately 5 times greater when irradiating ZnO/Au compared to ZnO. CPH is an often-used hole scavenger as it can be oxidized by holes.[35] To determine the specificity of CPH in detecting oxidants, we investigated the effects of the hydroxyl radical (generated by irradiating hydrogen peroxide), superoxide (produced by xanthine/XOD), and sodium azide on CPH oxidation (Supporting Information, Figures S5−S7). The results reveal that superoxide can induce CPH oxidation, but the hydroxyl radical and sodium azide (and therefore singlet oxygen) have a negligible effect on the CP· ESR signal. Also, the addition of SOD results in only a partial (~30%) reduction in the CP· ESR signal both for ZnO and ZnO/Au NPs (Supporting Information, Figure S8). These results indicate photoinduced holes and superoxide anion are the possible oxidants responsible for eliciting the CP· ESR signal, and with photogenerated holes being dominant.

The spin label TEMPO was selected for characterizing the electrons generated in photoexcited ZnO and ZnO/Au. TEMPO is a typical spin label molecule, having stable triplet ESR spectrum. It can be reduced (e.g., by electrons associated with photoexcited semiconductors) to give a hydroxyl amine (TEMPOH) which lacks an ESR signal.[31,36,37] Reduction of TEMPO is accompanied by flattening of the ESR signal (Figure 5). In our system, TEMPO does not react with oxidizing species (holes and ROS) or with unirradiated ZnO NPs. Importantly, superoxide anion has little effect on the ESR signal for TEMPO (Supporting Information, Figure S5). Therefore, under our experimental conditions, the formation of TEMPOH from TEMPO necessarily involves transfer of electrons from the surface of photoexcited ZnO or ZnO/Au surface to the spin label. Therefore, generation of photoinduced electrons and their reactivity can be easily monitored by observing changes in the ESR spectrum of TEMPO. The ESR spectrum of an aqueous solution of TEMPO shows a stable signal having three peaks with intensity of 1:1:1. The signal intensity was unchanged after mixing with catalysts before irradiation or irradiation without catalysts. The signal intensity decreased slightly within 5 min of irradiation in the presence of ZnO; however, a considerable reduction of ESR signal was observed during irradiation of ZnO/Au hybrid nanostructures (Figure 5). With extended irradiation times, more reduction was observed both for ZnO and ZnO/Au (data not shown). These results indicate that the electrons are produced from photoexcited ZnO and ZnO/Au NPs, and deposition of Au onto ZnO can greatly enhance the reactivity of the photoinduced electrons. This may be attributable to the low Fermi level of Au, resulting in the shuttling of conduction band electrons from ZnO to Au and increased availability of electrons for photoreductions.

Using ESR spectroscopy, we have demonstrated that hydroxyl radical, superoxide anion, and singlet oxygen are formed during

dx.doi.org/10.1021/ja410800y | J. Am. Chem. Soc. 2014, 136, 750−757

photoexcitation of ZnO and ZnO/Au. In addition, we have characterized the charge carriers generated during irradiation of these photocatalysts. Importantly, we also demonstrated that deposition of Au onto ZnO significantly enhances the photogeneration of all the identified reactive species. As mentioned above, ZnO/Au hybrid nanostructures with different Au/ZnO ratios could be synthesized controllably by changing the molar ratio of the reactants, $HAuCl_4$ and ZnO. The Au loading exhibited a profound influence on the photocatalytic activity of ZnO NPs. We investigated whether the levels of Au loading had similar effects on the photogeneration of each active species (hydroxyl radical, singlet oxygen, and electrons) (Figure 6). For BMPO and 4-oxo-TEMP, the ESR signal reflected the generation of hydroxyl radicals, superoxide and singlet oxygen, respectively. A similar dependence on Au loading was noted for both BMPO and 4-oxo-TEMP. An initial increase in the ESR signal intensity was noted for ZnO/Au hybrid nanostructures derived from reactant mixtures containing molar percentages of Au up to 2%, for BMPO, and 4%, for 4-oxo-TEMP. Diminishing ESR signal intensities were observed for ZnO/Au hybrid nanostructures having a higher molar percentage of Au. This decrease in ESR signal intensity for BMPO and 4-oxo-TEMP observed at higher levels of Au loading may be attributable to the SOD mimetic activity of Au NPs reported by us and others.[38] As we have demonstrated, the signal intensities of both BMPO and 4-oxo-TEMP are dramatically reduced in the presence of SOD (Supporting Information, Figures S3 and S9). At higher levels of Au loading, the SOD mimetic activity of the Au NPs deposited on ZnO may result in a net reduction of ESR signals for BMPO and 4-oxo-TEMP. For the spin label TEMPO, which was used to follow photogeneration of electrons, a similar dependence on the molar percentage of Au was observed. The photoreduction of TEMPO (as indicated by a decreasing TEMPO ESR signal) increased for ZnO/Au hybrid nanostructures derived from reaction mixtures containing a molar percentage of Au up to 4%. At higher levels of Au loading, the photoreduction of TEMPO decreased. For CPH, which was used to determine photooxidative behavior mainly caused by holes, a different trend was observed. The ESR signal of CP· increased quasi-linearly with increasing Au/ZnO ratio. These ESR results demonstrate that a similar dependence on Au content in the ZnO/Au hybrid structure is noted for BMPO, 4-oxo-TEMP, and TEMPO and could be used to detect and quantify hydroxyl radicals, singlet oxygen, and electrons generated as electron/hole pairs, respectively. A distinctly different dependence on Au loading was observed in the ESR results obtained for CPH, used to detect and quantify holes generated as electron/hole pairs. It is of interest to note that the ESR obtained for CPH and the photocatalytic activity have a similar dependence on levels of Au loading. This correlation between reactivity of holes and the photocatalytic activity suggests a mechanistic connection between light-induced generation of holes and photocatalytic activity. The results therefore suggest that photogenerated holes, rather than hydroxyl radicals, singlet oxygen, or electrons, play the dominant role in photocatalysis by ZnO/Au hybrid superstructures. It should be noted that gold NPs have been shown to be a catalyst for a variety of chemical reactions.[39] We have observed that Au nanodots themselves (ZnO/Au nanostructures without irradiation) have negligible ability in the generation of ROS and a very small contribution to the degradation of MB (about ~8%, data not shown).

Mechanism of Enhancement Effect of ZnO/Au Hybrid Nanostructures. As discussed above, when compared to ZnO, ZnO/Au hybrid nanostructures have enhanced activity in photogeneration of hydroxyl radicals, superoxide, singlet oxygen, photoinduced holes, and electrons. This enhancement in photogenerated reactive intermediates is consistent with the observed enhanced photocatalytic activity of ZnO/Au hybrid nanostructures. The mechanism for this enhancement may be understood by examining how Au, deposited on the surface of ZnO, affects the fate of photogenerated electrons and holes in ZnO. During irradiation of a semiconductor, electrons in the valence band are excited to the conduction band by the absorbed energy producing charge carriers. The electrons and holes have strong reductive and oxidative ability, respectively, and result in generation of reactive oxygen species. The valence band edge energy and conduction band edge energy of semiconductors determine the type of ROS generated during photoexcitation. The redox potential for dissolved oxygen/superoxide couple is −0.16 V ($E_0(O_{2(aq)}/O_2^{-\bullet})$), and for the $H_2O/\cdot OH$ couple is 2.32 V($E_0(H_2O/\cdot OH)$) at pH 7.[40] Therefore, photogenerated electrons, needed to form superoxide, must therefore have a potential less than −0.16, and photogenerated holes, needed to form hydroxyl radicals, must have a potential greater than 2.32. As shown in Figure 7a, ZnO, a wide band gap (E_g = 3.2 eV)

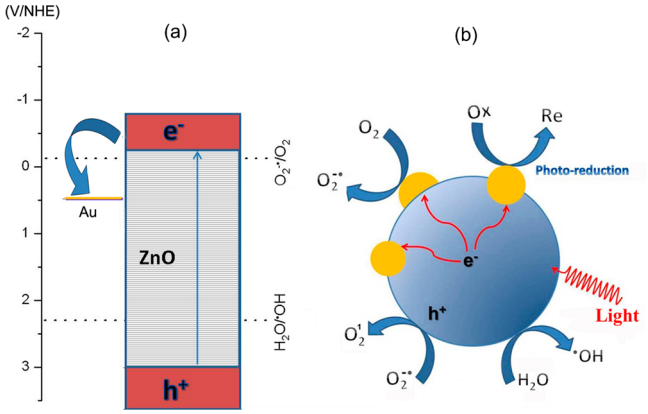

Figure 7. (a) Position of Fermi level of Au and energy bands of ZnO compared with redox potential of $O_2^{-\bullet}/O_2$ and $H_2O/\cdot OH$, (b) Expected reaction mechanism for enhancement effect on generation ROS and photocatalytic activity. Deposition of Au onto ZnO increases the charge carrier separation and transport efficiency in photoexcited ZnO NPs.

semiconductor, has a conduction band edge with redox potential of −0.2 V and a valence band edge with redox potential of 3.0 V.[41] Thus, the highly reactive holes react with water to generate hydroxyl radicals, and electrons react with dissolved oxygen to produce superoxide anions. We observed that more hydroxyl radicals are generated than superoxide anions during photoexcitation of ZnO or ZnO/Au hybrid nanostructures. This may be attributed to the higher redox potential difference (0.68 V) between the valence band edge and the $H_2O/\cdot OH$ couple than those (0.04 V) between the conduction band electrons and $O_{2(aq)}/O_2^{-\bullet}$.

We have previously reported that singlet oxygen is generated from photoexcited TiO_2 NPs, and that the mechanism involves a reaction between superoxide anions and holes.[42] Because of the similarity between ZnO and TiO_2, we propose that a similar mechanism underlies our current observations. To demonstrate this hypothesis, the effect of SOD on the singlet oxygen generation was studied. We found that the addition of SOD greatly reduced (~90%) the generation of singlet oxygen

dx.doi.org/10.1021/ja410800y | J. Am. Chem. Soc. 2014, 136, 750−757

measured using the spin probe, 4-oxo-TEMP (Supporting Information, Figure S9). These results indicate that the formation of singlet oxygen involves the intermediate formation of superoxide. In addition, neither superoxide nor hydroxyl radicals were found to react with 4-oxo-TEMP to give a signal expected for 4-oxo-TEMP reacting with singlet oxygen (Supporting Information, Figures S5 and S6). These results show the specificity of 4-oxo-TEMP for detecting singlet oxygen. Taken together, these results support the view that singlet oxygen, formed during irradiation of ZnO or ZnO/Au hybrid nanostructures, is the product of a reaction between superoxide and holes.

For the ZnO/Au hybrid nanostructures, the observed enhanced photocatalytic activity and ROS generation may result from the following possible effects of Au in the ZnO/Au hybrid nanostructures: (1) enhancing light absorption because of the SPR of Au, (2) changing the band gap of ZnO and thereby promoting reactivity of photoinduced charge carriers, and (3) increasing the efficiency of electron transport and charge carrier separation. As we discussed in the previous section, for the ZnO/Au hybrid nanostructures studied in this work, the Au dots smaller than 3 nm show very weak SPR. This indicates that increased absorption of light through the SPR of Au does not play a role in the enhanced photoactivity observed for the ZnO/Au hybrid nanostructures. In addition, we investigated the wavelength dependence for generation of ROS for ZnO and ZnO/Au hybrid nanostructures (Supporting Information, Figure S10). Although the hybrid structures show great enhancement for ROS generation, they have the same absorption spectrum between 200 and 450 nm and exhibit the same wavelength of maximum absorbance (near 350 nm) as the ZnO nanostructures. Wavelengths greater than 350 nm were ineffective in driving the generation of ROS. This indicates that deposition of Au onto ZnO does not significantly change the wavelengths of light which drive the generation of ROS. We also observed that deposition of Au dots onto ZnO results in a slight widening of the band gap. A widening of the band gap caused by Au deposition might result in the shift of the conduction band edge and valence band edge. The conduction band edge shift to more negative, or valence band edge move toward more positive, or both will happen. As a result, the reductive activity of electrons in conduction band or the oxidative ability of holes in valence band or both will be increased, which subsequently will enhance the generation of ROS. Therefore, band gap widening due to deposition of Au on ZnO may contribute to the enhancing effects observed for photocatalysis and generation of ROS. For the third effect, it has been demonstrated that Au NPs possess the property of storing electrons.[43] When the semiconductor and metal NPs are in contact, the photogenerated electrons are distributed between ZnO and Au NPs (Fermi level of Au +0.45 V versus NHE). The transfer of electrons from the excited ZnO into Au results in the higher separation efficiency of electrons and holes, and as a result, can enhance both generation of ROS and the photo-oxidation/reduction activity (Figure 7b). Therefore, changes in band gap and efficiency in electron transfer are the most probable reasons for the observed enhancement of photocatalytic activity and ROS generation resulting from deposition of Au on ZnO.

Enhanced Effect of Au on the Antibacterial Activity of ZnO/Au Hybrid Nanostructures. Our ESR results suggest that the biological activity of ZnO, such as antibacterial activity, can be enhanced by deposition of Au onto ZnO. To compare the antibacterial ability of ZnO and ZnO/Au hybrid nanostructures, two representative bacteria, gram positive *S. aureus* and gram negative *E. coli* were selected. Both the *S. aureus* and *E. coli* grew well in the absence of nanomaterials and irradiation (Figure 8, Control 1). Irradiation with simulated sunlight caused a decrease in bacterial survival (Control 2), exposure to NPs alone, without irradiation, resulted in decreased bacterial survival compared to untreated controls. With the addition of ZnO NPs, the survival of both *S. aureus* and *E. coli* decreased further when exposed to simulated sunlight for 10 min. This decrease may be attributed to ROS generated during photoexcitation of ZnO. We observed an enhancement in antibacterial activity for bacteria exposed to ZnO/Au hybrid nanostructures and simulated sunlight. For example, the ZnO/Au hybrid nanostructures were about 3 times more effective in killing *E. coli* than pure ZnO NPs. The observed antibacterial activity also increased with increased levels of ZnO or ZnO/Au (Figure 8). ZnO NPs have been considered as antimicrobial products especially when irradiated. The exact mechanism of antibacterial activity of ZnO is still unclear and may involve generation of ROS, release of Zn^{2+} ions and damage to cell membranes. While we cannot definitively describe the mechanism of antibacterial activity, our ESR results suggest that the dominant mechanism underlying Au enhancement of the antibacterial activity of photoexcited ZnO is the generation of ROS. Both the photocatalytic activity and antibacterial activity of photoexcited semiconductors have frequently been attributed to the generation of ROS. Additional studies are needed to determine the role of individual ROS in antibacterial activity of photoexcited ZnO/Au hybrid nanostructures because of the complexity in biological environments.

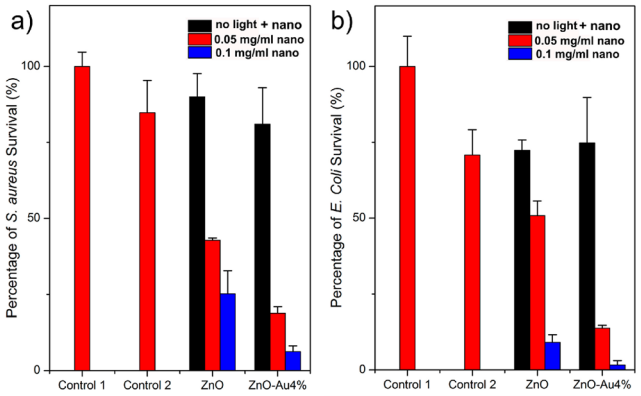

Figure 8. Ability of ZnO NPs and ZnO/Au hybrid nanostructures in killing *S. aureus* (a) and *E. coli* (b) under simulated sunlight for 10 min. Control 1 represents bacteria exposed to neither NPs nor light. Control 2 represents bacteria exposed to simulated sunlight for 10 min but without NPs. Grouped under ZnO, bacteria were exposed to 0.1 mg/mL ZnO alone or were exposed to 10 min of solar simulated light and either 0.05 mg/mL or 0.1 mg/mL ZnO. Similarly, grouped under ZnO–Au4%, bacteria were exposed to 0.1 mg/mL ZnO/Au4% alone or were exposed to 10 min of solar simulated light and either 0.05 mg/mL or 0.1 mg/mL ZnO/Au4%.

CONCLUSIONS

Small Au dots decorated on ZnO NPs exhibited significant enhancement of ROS generation, photocatalytic activity and broad antibacterial activity toward gram positive and gram negative bacteria. Using ESR spectroscopy with spin trapping and spin labeling, we definitively identified the ROS generated from ZnO and ZnO/Au hybrid nanostructures when excited with simulated sunlight. In addition, we determined that the

dx.doi.org/10.1021/ja410800y | J. Am. Chem. Soc. 2014, 136, 750−757

ZnO/Au hybrid nanostructures exhibited enhanced charge carrier reactivity. This enhancement effect may be attributed to a higher efficiency of electron transport and charge carrier separation induced by Au NPs. The enhanced ROS generation, photocatalytic and antibacterial activity of ZnO/Au hybrid nanostructures showed a distinctive Au/ZnO ratio dependence. These results not only provide an efficient method to identify and distinguish ROS and holes/electrons separately, but also demonstrate an effective way to improve photocatalytic and antibacterial activity of semiconductors by incorporation of metals.

■ ASSOCIATED CONTENT

Supporting Information

Experimental details and additional figures (Figures S1−S10) as described in the text. This material is available free of charge via the Internet at http://pubs.acs.org.

■ AUTHOR INFORMATION

Corresponding Author

junjie.yin@fda.hhs.gov

Notes

The authors declare no competing financial interest.

■ ACKNOWLEDGMENTS

W. He thanks the National Natural Science Foundation of China (Grant No. 21303153 and 61204009) and the Research Project of Basic and Advanced Technology of Henan Province (Grant No. 112300410106) for support. H. K. Kim thanks the support from the Korean Government Scholarship Program. This work was supported by a regulatory science grant under the FDA Nanotechnology CORES Program and by the Office of Cosmetics and Colors, CFSAN/FDA. The authors appreciate Dr. Yongbin Zhang in NCTR/ORA Nanotechnology Core Facility for his assistance with BET measurements and Prof. Zhi Zheng from Xuchang University for his kind discussions.

■ REFERENCES

(1) Epstein, H. A. *SKINmed.* **2011**, *9*, 109−110.
(2) Leung, Y. H.; Chan, C. M. N.; Ng, A. M. C.; Chan, H. T.; Chiang, M.W. L.; Djurisic, A. B.; Ng, Y. H.; Jim, W. Y.; Guo, M. Y.; Leung, F. C. C.; Chan, W. K.; Au, D. T. W. *Nanotechnology* **2012**, *23*, 475703.
(3) Xie, Y. P.; He, Y. P.; Irwin, P. L.; Jin, T.; Shi, X. *Appl. Environ. Microbiol.* **2011**, *77*, 2325−2331.
(4) Chen, X.; Mao, S. S. *Chem. Rev.* **2007**, *107*, 2891−2959.
(5) Kubacka, A.; Fernández-García, M.; Colón, G. *Chem. Rev.* **2012**, *112*, 1555−1614.
(6) Chen, C. C.; Ma, W. H.; Zhao, J. C. *Chem. Soc. Rev.* **2010**, *39*, 4206−4219.
(7) Tamaki, Y.; Hara, K.; Katoh, R.; Tachiya, M.; Furube, A. *J. Phys. Chem. C* **2009**, *113*, 11741−11746.
(8) Costi, R.; Saunders, A. E.; Banin, U. *Angew. Chem., Int. Ed.* **2010**, *49*, 4878−4897.
(9) Murdoch, M.; Waterhouse, G. I. N.; Nadeem, M. A.; Metson, J. B.; Keane, M. A.; Howe, R. F.; Llorca, J.; Idriss, H. *Nat. Chem.* **2011**, *3*, 489−492.
(10) Peralta, M. D. L. R.; Pal, U.; Zeferino, R. S. *ACS Appl. Mater. Interfaces* **2012**, *4*, 4807−4816.
(11) Bian, Z. F.; Tachikawa, T.; Kim, W.; Choi, W.; Majima, T. *J. Phys. Chem. C* **2012**, *116*, 25444−25453.
(12) Fan, F. R.; Ding, Y.; Liu, D. Y.; Tian, Z. Q.; Wang, Z. L. *J. Am. Chem. Soc.* **2009**, *131*, 12036−12037.
(13) Lee, Y.; Garcia, M. A.; Frey Huls, N. A.; Sun, S. *Angew. Chem., Int. Ed.* **2010**, *49*, 1−5.
(14) Dukovic, G.; Merkle, M. G.; Nelson, J. H.; Hughes, S. M.; Alivisatos, A. P. *Adv. Mater.* **2008**, *20*, 4306−4311.
(15) Lee, J.; Shim, H. S.; Lee, M.; Song, J. K.; Lee, D. J. *Phys. Chem. Lett.* **2011**, *2*, 2840−2845.
(16) Atwater, H. A.; Polman, A. *Nat. Mater.* **2010**, *9*, 205−213.
(17) Liu, Z.; Hou, W.; Pavaskar, P.; Aykol, M.; Cronin, S. B. *Nano Lett.* **2011**, *11*, 1111−1116.
(18) Mubeen, S.; Lee, J.; Singh, N.; Kramer, S.; Stucky, G. D.; Moskovits, M. *Nat. Nanotechnol.* **2013**, *8*, 247−251.
(19) Rajendran, V.; Lehnig, M.; Niemeyer, C. M. *J. Mater. Chem.* **2009**, *19*, 6348−6353.
(20) Hoffmann, M. R.; Martin, S. T.; Choi, W.; Bahnemann, D. W. *Chem. Rev.* **1995**, *95*, 69−96.
(21) Fang, F. C. *mBio* **2011**, *2*, e00141−11.
(22) Brynildsen, M. P.; Winkler, J. A.; Spina, C. S.; MacDonald, I. C.; Collins, J. J. *Nat. Biotechnol.* **2013**, *31*, 160−165.
(23) Huang, Z.; Zheng, X.; Yan, D.; Yin, G.; Liao, X.; Kang, Y.; Yao, Y.; Huang, D.; Hao, B. *Langmuir* **2008**, *24*, 4140−4144.
(24) Heinlaan, M.; Ivask, A.; Blinova, I.; Dubourguier, H. C.; Kahru, A. *Chemosphere* **2008**, *71*, 1308−1316.
(25) Zhang, H.; Ji, Z.; Xia, T.; Meng, H.; Kam, C. L.; Liu, R.; Pokhrel, S.; Lin, S.; Wang, X.; Liao, Y. P.; Wang, M.; Li, L.; Rallo, R.; Damoiseaux, R.; Telesca, D.; Mädler, L.; Cohen, Y.; Zink, J. I.; Nel, A. E. *ACS Nano* **2012**, *6*, 4349−4368.
(26) Zhang, W.; Li, Y.; Niu, J.; Chen, Y. *Langmuir* **2013**, *29*, 4647−4651.
(27) Hirakawa, T.; Kominami, H.; Ohtani, B.; Nosaka, Y. *J. Phys. Chem. B* **2001**, *105*, 6993−6999.
(28) Tang, J.; Durrant, J. R.; Klug, D. R. *J. Am. Chem. Soc.* **2008**, *130*, 13885−13891.
(29) Norris, J. R.; Uphaus, R. A.; Crespi, H. L.; Katz, J. J. *Proc. Natl. Acad. Sci. U.S.A.* **1971**, *68*, 625−628.
(30) Jaeger, C. D.; Brad, A. J. *J. Phys. Chem.* **1979**, *83*, 3146−3152.
(31) Schrauben, J. N.; Hayoun, R.; Valdez, C. N.; Braten, M.; Fridley, L.; Mayer, J. M. *Science* **2012**, *336*, 1298−1301.
(32) Hu, M.; Chen, J.; Li, Z.; Au, L.; Hartland, G. V.; Li, X.; Marqueze, M.; Xia, Y. *Chem. Soc. Rev.* **2006**, *35*, 1084−1094.
(33) Hubbell, W. L.; McConnell, H. M. *Proc. Natl. Acad. Sci. U.S.A.* **1968**, *61*, 12−16.
(34) Zhao, H. T.; Joseph, J.; Zhang, H.; Karoui, H.; Kalyanaraman, B. *Free Radic. Biol. Med.* **2001**, *3*, 599−606.
(35) Tanaka, A.; Sakaguchi, S.; Hashimoto, K.; Kominami, H. *ACS Catal.* **2013**, *3*, 79−85.
(36) Zhou, Z.; Zhang, Z. *Chin. J. Magn. Reson.* **1999**, *2*, 89−95.
(37) Zhou, Z.; Liu, W.; Wang, F.; Zhang, Z. *Sci. China (C)* **2001**, *44*, 241−252.
(38) He, W. W.; Zhou, Y.; Wamer, W. G.; Hu, X. N.; Wu, X. C.; Zheng, Z.; Boudreau, M. D.; Yin, J. J. *Biomaterials* **2013**, *34*, 765−773.
(39) Haruta, M.; Daté, M. *Appl. Catal. A: Gen.* **2001**, *222*, 427−437.
(40) Wood, P. M. *Biochem. J.* **1988**, *253*, 287−289.
(41) Nozik, A. J.; Memming, R. *J. Phys. Chem.* **1996**, *100*, 13061−13078.
(42) Yin, J. J.; Liu, J.; Ehrenshaft, M.; Roberts, J. E.; Fu, P. P.; Mason, R. P.; Zhao, B. *Toxicol. Appl. Pharmacol.* **2012**, *263*, 81−88.
(43) Subramanian, V.; Wolf, E. E.; Kamat, P. V. *J. Phys. Chem. B* **2003**, *107*, 7479−7485.